Comparative OHD-RIKES and THz-TDS Probes of Ultrafast Structural Dynamics in Molecular Liquids

Matthew C. Beard,[†] William T. Lotshaw,*[,‡] Timothy M. Korter,[§] and Edwin J. Heilweil

National Institute of Standards and Technology, Gaithersburg, Maryland 20899

Dale McMorrow

Naval Research Laboratory, Code 6812, Washington, D.C. 20375

Received: June 7, 2004; In Final Form: August 5, 2004

We compare terahertz time domain (THz-TDS) and optical heterodyne-detected Raman-induced Kerr effect (OHD-RIKES) spectroscopic techniques as probes of molecular and vibrational dynamics in the frequency range of 0.1 to 6 THz (3 to 200 cm^{-1}). The spectra of molecular liquids benzene, toluene, and bromobenzene, with dipole moments in the range of 0 to 1.7 D, are analyzed within a multimode spectral decomposition to examine the relative sensitivities of the techniques to distinguishable dynamical coordinates. We emphasize the use of minimum modal bases primarily for the purpose of comparing the spectra. Significant differences are found between the THz and OHD-RIKES spectra of benzene and bromobenzene that cannot be traced to rescaled oscillator strengths within a set of fixed-frequency modes.

Introduction

A detailed understanding of the microscopic structure and dynamics of molecular liquids and solids has important scientific and technological justifications: as a milieu for chemical reactions, the molecular and structural dynamics of liquids affect the rate and magnitude of the solvent dielectric response to charged or polar reaction intermediates.[1] Similarly, thermal or strain-induced structural relaxations in polymer glasses degrade functional properties in, for example, guest−host electrooptic materials[2] via the loss of imposed spatial configurations of active dopants. The prospects for control and optimization of materials in these types of applications are premised upon an intimate knowledge of the correlation between chemical properties and structural dynamics. The acquisition of such an understanding is necessarily contingent on the ability to measure the dynamics sensitively over as large a range of time and frequency as possible, thereby allowing refinement and validation of theoretical models. Various spectroscopic techniques have been enlisted in the pursuit of such measurements: dielectric loss spectroscopy[3], NMR,[4] dynamic light scattering[5] (DLS), transient absorption[6] and fluorescence,[7] and nonlinear optical spectroscopy.[8] These techniques have been used to identify and interrogate molecular, intermolecular, and collective degrees of freedom. Over the past 15 years, femtosecond optical Kerr spectroscopy in the form of the optical heterodyne-detected Raman-induced Kerr effect (OHD-RIKES) has emerged as a method of choice for probing vibrational and molecular dynamics over ∼5 orders of magnitude in time and frequency,[9,10] from a few femtoseconds to hundreds of nanoseconds and 0.1 GHz to ∼20 THz, respectively. The objective of uniquely tracing the highly resolved dynamics observed by the OHD-RIKES technique to specific intermolecular interactions has spawned studies over wide ranges of temperature[10−12] and number density[13,14] in molecular liquids. Similarly, OHD-RIKES has been applied in the continuing effort to trace bulk thermo-mechanical properties in glasses[10] and liquid crystals[15,16] to the unique nonlinear constraints on molecular and supramolecular degrees of freedom in those systems. Taken in conjunction, these applications probe interactions and dynamics on length scales ranging from submolecular to effectively bulk dimensions.

Particular spectroscopic techniques are sensitive to specific electronic properties of materials; therefore, it is useful (if not necessary) to validate models of molecular dynamics that are tested primarily using one experimental technique with complementary measurements using another. To this end, the molecular dynamics of solvents measured by OHD-RIKES have previously been compared to the dynamic fluorescence Stokes shift of fluorophores in solution, which probes the dielectric relaxation of the solvent−solute system.[1] That comprehensive review concluded that although no simple relationship was seen between the two measurements, the discrepancies were traceable to the specific sensitivities of the probes: OHD-RIKES being more sensitive to short-range interactions between solvent molecules, whereas the dynamic Stokes shift reveals interactions between an electronically excited solute and the surrounding solvent. Alternately, terahertz time-domain spectroscopy[17] (THz-TDS) has a reliable frequency range in the far-infrared (FIR) of ∼0.1 to ∼10 THz (dependent upon the emitter/detector technology) that is well matched to that of OHD-RIKES and to the frequency range of molecular and structural dynamics in liquids and glasses (≤20 THz, or Raman shifts ≤700 cm^{-1}). Because THz-TDS probes the dipolar properties of materials over the same frequency range that OHD-RIKES probes the polarizability, the tandem use of these techniques offers a potential for interrogations of molecular motion and intermolecular interactions at much greater depth than is possible by either technique alone.

* Corresponding author. E-mail: wtlotshaw@msn.com.
[†] NRC Postdoctoral Fellow. Current address: National Renewable Energy Laboratory, Golden, CO 80401.
[‡] NIST Guest Researcher. Current address: Contractor, Naval Research Laboratory, Code 6812, Washington, DC 20375.
[§] NIST Guest Researcher. Current address: Department of Chemistry, Syracuse University, Syracuse NY 13244-4100.

10.1021/jp047547a CCC: $27.50
Published on Web 10/01/2004

That proposal was investigated by Rønne et al.[18] using THz-TDS and OHD-RIKES to examine the temperature-dependent molecular dynamics of the nonpolar liquid benzene. The spectral densities measured by the two techniques were compared in the range of ~0.2 to 3.3 THz (~7 to 110 cm^{-1}). A higher spectral amplitude and a distinct temperature dependence in the 0.4−1.8 THz frequency range was observed in the THz measurements. The differences were attributed to three-body effects on the in-plane libration of benzene about its symmetry axis, a coordinate to which the OHD-RIKES probe is insensitive to first order. These conclusions were investigated further via molecular dynamics simulations,[19] which buttressed and refined the proposal that the in-plane motion of the quadrupole-induced dipole moment is more sensitive to three-body interactions than the out-of-plane motions at higher and lower frequencies, thereby accounting for the difference between the spectra. That seminal work[18] exhibited two potential liabilities: the experimental frequency range was significantly narrower than the spectral band being studied, and the OHD-RIKES data were modified in a way that alters the associated spectral density in the range where the largest discrepancy was noted (0.4−1.8 THz). A more recent report investigated the general correspondence of OHD-RIKES and far-infrared (FIR) probes of polar and hydrogen-bonding liquids within a multimode Brownian oscillator analysis of the respective spectral densities.[20] In that work the FIR spectra were reconstructed from two distinct THz-TDS measurements at frequencies ≤80 cm^{-1} plus FTIR data in the range of 80−150 cm^{-1}; five terms were typically required to fit the spectral density in the range of 0−150 cm^{-1}.

In this report, we reexamine the correspondence of OHD-RIKES and THz-TDS probes of molecular dynamics in benzene, toluene, and bromobenzene in the frequency range of ~0.1 to ~4.5 THz (~3 to 150 cm^{-1}). This limited sample set was selected for the serial variation in dipole moment[21] (0 D for benzene, 0.36 D for toluene, and 1.70 D for bromobenzene), its relative chemical simplicity, and the existence of recent OHD-RIKES and THz-TDS data from other laboratories.[12,18−20] Our objective is to investigate the basis for using OHD-RIKES and THz-TDS spectroscopy as complementary probes capable of distinguishing theoretically separable intermolecular interactions and dynamics in the condensed phase. Such complementary characterization tools are necessary to validate physical models objectively and thereby generate unique interpretations of spectroscopic information. In particular, we will examine the consequences of data reduction methods commonly used to acquire the OHD-RIKES spectral density and the use of multimode spectral decompositions for interpretation of the relatively featureless spectra arising from molecular and intermolecular coordinates in liquids and glasses.

Experimental Methods

THz-TDS. The FIR absorption measurements were made utilizing a THz-TDS spectrometer for frequencies from ~5 to 130 cm^{-1} and a modified Fourier transform infrared spectrometer (FTIR) for the range of 75 cm^{-1} to 400 cm^{-1} (Nicolet Magna 550[22] with a Si-coated beam splitter and room-temperature DTGS detector fitted with a polyethylene window). For the THz-TDS measurements, terahertz frequency generation occurs via nonresonant optical rectification of an 800 nm, 90 fs fwhm laser pulse in a 150-μm-thick ⟨110⟩ GaP crystal. The 800-nm pulses are generated in a home-built, regeneratively amplified Ti:sapphire laser operating at 1-kHz repetition rate and ~700-μJ output pulse energy. The seed oscillator is a CW-pumped, Kerr-lens modelocked Ti:sapphire laser (Kapteyn-Murnane Laboratories, Boulder, CO[22]) that delivers a 40-fs fwhm pulse duration seed to the amplifier. A schematic diagram of the THz-TDS spectrometer is shown in Figure 1.

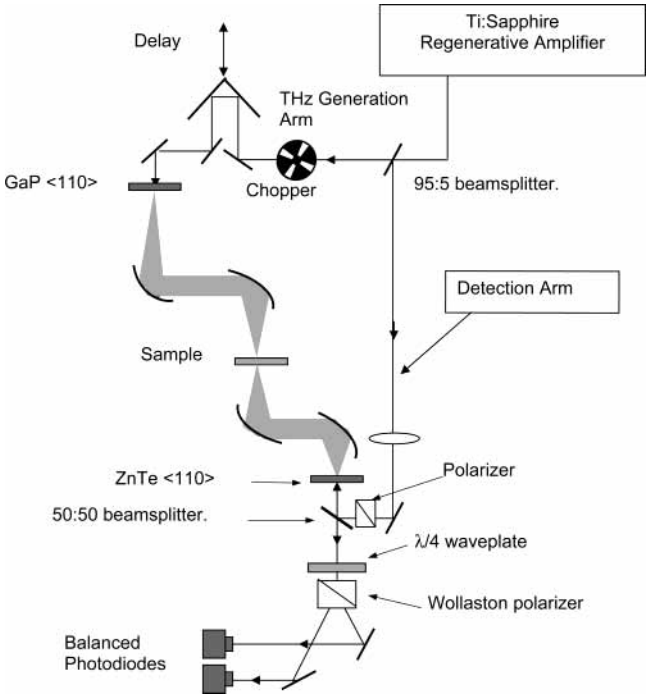

Figure 1. Experimental TDS-THz spectrometer.

The details of the experimental protocol have been described previously;[17] here, we will only note deviations from established procedures. A small portion of the amplified 800-nm pulse was split off and delayed with respect to the THz generation arm for the detection of the THz pulse via free-space electrooptic sampling[23] in a 500-μm-thick ⟨110⟩ ZnTe crystal. The ZnTe detector crystal served a dual purpose as a beam combiner to couple the 800-nm read-out beam into the THz beam path via reflection off of the front crystal surface. Figure 2 shows a typical THz transient and power spectrum, containing frequency components from ~5 cm^{-1} to ~130 cm^{-1} (~0.15 to 4 THz). The GaP generator and ZnTe detector combination yielded a substantially broader spectral range than a ZnTe generator/detector combination. The samples were placed in a variable path length cell with 2-mm-thick and 25-mm diameter polyethylene windows. The path length was established by Teflon spacers of known thickness and measured via the round-trip transit time of a reference THz pulse. The reference THz transients were collected with the empty sample cell in the THz beam path, which was vigorously purged with dry air prior to data collection to reduce absorption due to water vapor. An optical chopper that was phase locked to the laser repetition rate modulated the generation arm at ~125 Hz, and a lock-in amplifier with an analog/digital converter was used to collect the data. At least three data sets were collected for each liquid at 21 °C, each set consisting of several sample path lengths and an empty cell reference scan. Spectral distortion at low frequency due to "windowing" by the sample cell is minimized by the large cell diameter, careful registration of the cell location during sample and reference data scans, and the data reduction procedure for the sample and reference signals described below.

One of the advantages of the THz-TDS technique is that the full electric field is measured in the time domain; thus, both the real and imaginary parts of the complex permittivity, $\epsilon(\omega) = \epsilon'(\omega) + i\epsilon''(\omega)$ (or equivalently the absorption coefficient $\alpha(\omega)$ and index of refraction $n(\omega)$) are measured simultaneously,

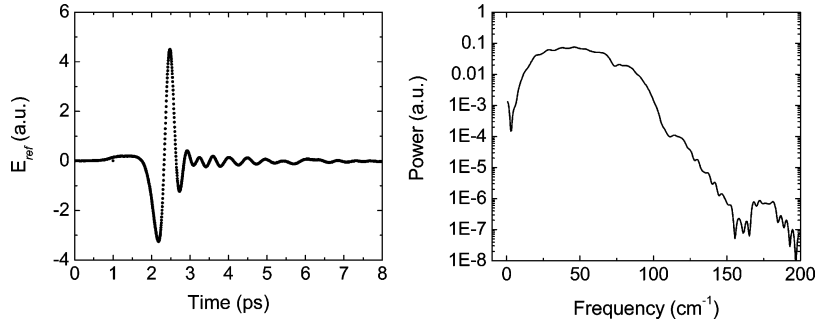

Figure 2. Left panel is a typical time-domain THz reference transient. Right panel is the associated power spectrum.

where ω is the angular frequency ($\omega = 2\pi\nu$). THz waveforms are measured in the time domain, giving $\hat{E}_{\mathrm{THz}}(t, d)$ where d is the thickness of the cell. The data at constant path length varied by no more than 3% over the scan range, and the data sets for each liquid were averaged to generate the $\hat{E}_{\mathrm{sample}}(t, d)$ used in subsequent numerical analyses. The frequency domain representation, $\hat{E}_{\mathrm{sample}}(\omega, d)$, is obtained from $\hat{E}_{\mathrm{sample}}(t, d)$ by Fourier transformation. To extract the optical constants with minimal spectral distortion, the transmitted pulse, $\hat{E}_{\mathrm{sample}}(\omega, d)$, is divided by the reference pulse, $\hat{E}_{\mathrm{ref}}(\omega, d)$, resulting in the complex transmission coefficient

$$\hat{T}_{\mathrm{meas}}(\omega, d) = \frac{E_{\mathrm{sample}}(\omega, d)}{E_{\mathrm{ref}}(\omega, d)} \tag{1}$$

This ratio is related to the change in optical density (ΔOD) and change in phase ($\Delta\phi$) by

$$\Delta OD = -\log\left(\frac{|E_{\mathrm{sample}}(\omega, d)|^2}{|E_{\mathrm{ref}}(\omega, d)|^2}\right) = -\log\left(|\hat{T}_{\mathrm{meas}}|^2\right) \tag{2}$$

and

$$\Delta\phi = \phi_{\mathrm{sample}} - \phi_{\mathrm{ref}} \tag{3}$$

where $\phi = \arctan(\mathrm{Im}[\hat{E}(\omega,d)]/\mathrm{Re}[\hat{E}(\omega,d)]$. The relationship between $\hat{T}(\omega)$ and complex wavevector $k(\omega)$ is

$$\hat{T} = \frac{k_{\mathrm{s}}(k_{\mathrm{air}} + k_{\mathrm{win}})^2}{k_{\mathrm{air}}(k_{\mathrm{s}} + k_{\mathrm{win}})^2}\exp[i(k_{\mathrm{s}} - k_{\mathrm{ref}})d] \tag{4}$$

where the explicit dependence on ω has been omitted for clarity. The wavevector k is related either to $\epsilon'$and ϵ'' or α and n by

$$k(\omega) = \frac{2\pi n(\omega)}{\lambda} + i\frac{\alpha(\omega)}{2} = \frac{2\pi\sqrt{\epsilon'(\omega) + i\epsilon''(\omega)}}{\lambda} \tag{5}$$

where k_{s}, k_{air}, and k_{win} are the sample, air, and polyethylene window wavevectors, respectively. The wavelength is λ, and the values $n_{\mathrm{air}} = 1$, $\alpha_{\mathrm{air}} = 0$, $n_{\mathrm{win}} = 1.5$, and $\alpha_{\mathrm{win}} = 0$ were used. Because eq 4 cannot be inverted analytically to obtain k_{s} as a function of the measured quantity, $\hat{T}_{\mathrm{meas}}$, a numerical inversion is performed at each frequency employing a Newton−Raphson algorithm.[24] The preexponential factor in eq 4 accounts for losses due to the different reflectivity of the air−polyethylene interfaces compared to the sample−polyethylene interfaces. During data collection, any reflections resulting from the sample windows, sample compartment, and detector crystal were windowed out of the data; as a result, eq 4 is applicable only in the so-called "thick film" limit. The result of this windowing in the time domain restricts the frequency resolution to $\sim$3 cm^{-1} ($\sim$0.1 THz).

The FTIR data were collected in the same sample cell described above for the THz-TDS measurements and referenced to an empty cell. The data were collected at a resolution of 4 cm^{-1} to avoid Etalon effects from multiple reflections in the cell. The resulting data contain usable frequencies from 75 to 400 cm^{-1}, but the data is truncated at 200 cm^{-1} for this work. The absorption coefficient obtained from the FTIR and THz-TDS data sets were overlapped in the frequency range from 75 to 120 cm^{-1}. A Kramers−Kronig transformation was performed on the resulting data over the combined spectral range of 5 to 400 cm^{-1} to obtain the index of refraction in the range of 120−200 cm^{-1}.

The imaginary part of the complex permittivity is related to the Fourier transform of the dipole correlation function by

$$\epsilon''(\omega) = \frac{4\pi^2}{3\hbar V}\left[1 - \exp\left(\frac{-\hbar\omega}{k_{\mathrm{B}}T}\right)\right]\frac{1}{2\pi}\int_{-\infty}^{\infty}\langle M(t)\, M(0)\rangle \exp(-i\omega\, t)\mathrm{d}t \tag{6}$$

where $M(t)$ is the total dipole moment operator and V is the sample volume. Because the principal objective of this report is to compare the spectral densities for molecular and intermolecular coordinates measured by the THz-TDS and OHD-RIKES techniques, we adopt $\epsilon''(\omega)$ and $\chi^{(3)}_{\mathrm{eff}}(\omega)$, the imaginary part of the Raman susceptibility, as corresponding quantities.[18,19] The reasons for this convention[18] are that these quantities relate most directly to the dynamical properties of interest (the time-correlation functions for the dipole moment and polarizability). In contrast, use of FIR absorptivity α imparts a frequency bias to the FIR data and subsequent spectral analyses via the relation

$$\alpha(\omega) = \frac{\omega\epsilon''(\omega)}{cn(\omega)} \tag{7}$$

where c is the speed of light and $n(\omega)$ is the frequency dependent refractive index. The most transparent deficit of the $\alpha(\omega)$ representation (and direct measurements of FIR absorptivity) is the suppression of low-frequency spectral detail, which obscures the observation and analysis of orientational diffusion degrees of freedom.[18]

OHD-RIKES. The procedures of the OHD-RIKES experiment have been described in detail previously.[9,13] The temperature of the samples was held constant in a TEC-regulated fixture using a PID controller and thermistor calibrated against the melting and boiling temperatures of high-resistivity distilled and deionized water. The liquid samples were of the highest purity available from Sigma-Aldrich, and were filtered in Whatman UniPrep PTFE syringeless filters to remove particulate

contaminants (>0.2 μm) prior to use. The sample cells were Teflon-stoppered fused silica with a 2-mm path length.

The laser system used for these experiments was a synchronously pumped Ti:Sapphire oscillator that generates transform-limited ≤40-fs fwhm pulses at a 76-MHz repetition rate and ≥750 mW of average power (~10-nJ pulse energy).[25] The laser wavelength was tunable and was set to ~800 nm. Data acquisition followed our previously established protocols.[9,13] For each liquid studied, five consecutive scans were averaged to generate the time-domain response function used in subsequent numerical analyses. The experimental response functions are typically analyzed for contributions from diffusive molecular reorientation at times greater than ~2−3 ps and over a temporal range of at least 2 time constants by linear least-squares fitting of the first order "tail" of the response function. These degrees of freedom exhibit decay constants that scale with temperature according to the Debye−Stokes−Einstein relation ($\tau_{or} \propto \eta/T$), and their contribution can be removed from the OHD-RIKES data by a previously described procedure[26] to focus attention on the underlying vibrational dynamics. However, for the purpose of comparison to the THz-TDS measurement in this report, the orientational diffusion contributions were not removed from the OHD-RIKES data.

The comparison of data measured by the OHD-RIKES and THz-TDS techniques is most direct in the frequency domain. The transformation of OHD-RIKES data into the frequency domain is accomplished by previously established methods,[9,26] which are briefly reviewed below. The relationship between the OHD-RIKES experimental data and material properties is given by[9,26]

$$T(\tau) = G_o^{(2)}(\tau) * R_{eff}^{(3)}(\tau), \tag{8}$$

where $T(\tau)$ is the measured time-domain response function of the Kerr cell, $G_o^{(2)}(\tau)$ is the laser pulse autocorrelation function, $R_{eff}^{(3)}(\tau)$ is the material response function, * represents the convolution operation, and τ is the time delay of the pump−probe pulse pair. $R_{eff}^{(3)}(\tau)$ is the third-order nonlinear optical response function for the optical Kerr effect and can be traced to the time-correlation function for the polarizability anisotropy of the sample medium.[27] $G_o^{(2)}(\tau)$ is independently measurable at the sample position by replacing the fluid cell with a thin nonlinear crystal such as KD*P. Fourier transformation of eq 8 gives

$$\mathcal{F}\{T(\tau)\} = \mathcal{F}\{G_o^{(2)}(\tau) * R_{eff}^{(3)}(\tau)\} = \mathcal{F}\{G_o^{(2)}(\tau)\} \times \mathcal{F}\{R_{eff}^{(3)}(\tau)\} \tag{9}$$

by the Fourier convolution theorem, and the deconvolved frequency dependent response function can be determined from the quotient of Fourier transforms of the experimentally measured quantities

$$\chi_{eff}^{(3)}(\omega) = \mathcal{F}\{R_{eff}^{(3)}(\tau)\} = \frac{\mathcal{F}\{T(\tau)\}}{\mathcal{F}\{G_o^{(2)}(\tau)\}} \tag{10}$$

where $\chi_{eff}^{(3)}(\omega)$ is the frequency-dependent Raman susceptibility (ω is typically reported in units of wavenumber) and $\mathcal{F}$ represents the (fast) Fourier transform operation.

The spectral densities measured by OHD-RIKES show remarkable correspondence in a wide variety of polar and nonpolar molecular liquids;[9,12,28] all exhibit a broad, relatively structureless band with a mean frequency in the range of 25−90 cm^{-1} and bandwidth in the 20−70 cm^{-1} range. In hydrogen-bonding liquids, the spectrum can extend to higher frequencies[29,30] (~200−350 cm^{-1}) and, in some cases, becomes more structured with two or more well-resolved bands. The spectral density in the 0−200-cm^{-1} range has been attributed to localized intermolecular coordinates defined by the relative positions and orientations of pairs or small aggregates of molecules. The bands show a complex dependence on temperature[12] and number density,[13,14] which is the object of continuing research.[12,14] The spectral density deduced by the OHD-RIKES technique can be measured directly in the frequency domain by stimulated Raman gain spectroscopy[31] and corresponds to the Rayleigh "wing" seen in DLS.[32]

Data Analysis. To examine the correspondence between OHD-RIKES and THz-TDS, we fit $\chi_{eff}^{(3)}(\omega)$ and $\epsilon''_j(\omega)$ spectra of bromobenzene, benzene, and toluene to a minimum number of Lorentzian, Gaussian, and collision-induced[33] (CI) functions. Different linear combinations of these functions were tested for their ability to fit the experimentally measured spectra. Fitting was accomplished using a nonlinear least-squares algorithm with a χ^2 criterion for goodness of fit.[24] The number of terms in each combination were iterated to determine the minimum needed to fit the experimental spectra; the minimum will be referred to as the basis for that combination. In this report, a Lorentzian is used to model the homogeneously broadened orientational diffusion coordinate closest to the frequency origin and in the overdamped limit, corresponds to the solution for the equation of motion of a damped, driven harmonic oscillator

$$\chi(t) = G_j \exp[-(\gamma_j - \beta_j)t](1 - \exp(-2\beta_j t)) \tag{11}$$

where γ_j is the damping coefficient, $\beta_j = \sqrt{\gamma_j^2 - \omega_j^2}$ is the angular velocity of the jth damped oscillator whose intrinsic (undamped) angular velocity is ω_j. The response function constants are lumped in G_j, which represents a coupling term that accounts for oscillator strength. For overdamped oscillators ($\gamma_j > \omega_j$), eq 11 has a $^1/_e$ decay time of $1/(\gamma_j - \beta_j)$ and a rise time of $1/(2\beta_j)$. A Laplace−Fourier transform of eq 11 results in the frequency domain representation given by

$$\chi_j(\omega) = \frac{G_j}{(\gamma_j - i\omega)^2 - \beta_j^2} \qquad \chi_j(\nu) = \frac{G_j}{(\gamma'_j - i\nu)^2 - \beta'^2_j} \tag{12}$$

where $\gamma_j = 2\pi\gamma'_j$, $\beta_j = 2\pi\beta'_j$, and $\omega = 2\pi\nu$. In the above equations, χ is the dielectric susceptibility related to the imaginary part of the complex permittivity by

$$\mathrm{Im}\{\chi_j\} = \epsilon''_j(\omega) = \frac{2G_j\omega\gamma_j}{(\gamma_j^2 + \omega^2)^2 - 2\beta^2(\gamma_j^2 - \omega^2) + \beta^4};$$

$$\epsilon''_j(\nu) = \frac{2G_j\nu\gamma'_j}{(\gamma'^2_j + \nu^2)^2 - 2\beta'^2(\gamma'^2_j - \nu^2) + \beta'^4} \tag{13}$$

We note that the Lorentzian function defined above is commonly used to represent homogeneously broadened vibrational transitions in Brownian oscillator analyses of vibrational spectra.[34] Our use of the Lorentzian function to describe diffusive reorientation coordinates is consistent with such analyses. For bases containing more than one Lorentzian, the higher-frequency terms represent unspecified intermolecular vibrational coordinates that could correspond to the CI or Gaussian terms of the other bases. These cases will be discussed individually.

Gaussian and collision-induced (CI) functions are used to model inhomogeneously broadened intermolecular coordinates

at higher frequency. The spectral density of the CI contribution is represented by

$$g_j(\omega, \alpha_j) = \omega^{\alpha_j} \exp\frac{-\omega}{\omega_j} \quad (14)$$

This expression was developed to account for the amplitude at intermediate frequencies in the Rayleigh wing of DLS spectra.[33] The parameter α_j is traceable to the exponent of the pairwise intermolecular separation $\hat{r}_{kl}$ in the intermolecular potential, and $\alpha_j\omega_j$ is taken to be the center frequency, where the derivative of eq 14 with respect to ω is zero. Although values for α_i in the range of $1 \leq \alpha_i \leq 1.8$, which focus on effects due to the repulsive part of the intermolecular potential, have become canonical in the application of eq 14 to modal analyses of vibrational spectra,[28] values of $\alpha_i < 1$ are not disallowed and correspond[33] to intermediate-range intermolecular interactions traceable to potential functions that vary with $\hat{r}_{kl}$ in the range of r^{-7} to r^{-9}. We have previously employed the Gaussian as an inhomogeneous line shape function for molecular libration at frequencies ≥ 20 cm^{-1}.[14] To satisfy the constraint on the spectral density of zero cross-section at zero frequency, we employ the antisymmetrized Gaussian function given by

$$g_j(\omega) = G_j\left[\exp\left[\frac{-(\omega - \omega_j)^2}{\sigma_j^2}\right] - \exp\left[\frac{-(\omega + \omega_j)^2}{\sigma_j^2}\right]\right] \quad (15)$$

where σ_j is related to the fwhm by $\sigma_{\text{fwhm}} = \sigma 2\sqrt{\ln 2}$. In basis sets that included the Gaussian function, it was used as the highest-frequency term to obtain the best quality of fit at frequencies > 80 cm^{-1}.

Except where noted, the fitting procedure for $\chi^{(3)}_{\text{eff}}(\omega)$ spectra is constrained such that the $^1/_e$ lifetime parameter $[1/(\gamma_i - \beta_i)]$ of the lowest-frequency Lorentzian (eqs 11 and 12) must replicate the lifetime for orientational diffusion (τ_{or}) measured in the time-domain OHD-RIKES data. The fitting procedure for $\epsilon''_j(\omega)$ spectra is similarly constrained by the lifetime that is expected for the dipolar time-correlation function on the basis of the OHD-RIKES orientational diffusion lifetime (vide infra). Because the $\epsilon''_j(\omega)$ data record stops at $\sim$4 cm^{-1}, we anticipate that the orientational diffusion parameters fitted to the THz-TDS data will be generally less reliable than those resulting from fits to the $\chi^{(3)}_{\text{eff}}(\omega)$ data, which extend to zero frequency. The basis combinations that resulted in the best fits consisted of (1) two Lorentzians and a Gaussian function (L−L−G), (2) a Lorentzian, a CI, and a Gaussian function (L−CI−G), and (3) all Lorentzians (up to 5 terms). In the tables, the functional terms are listed in the order of increasing center frequency in each basis.

In the tables, we report the standard deviation of the fitted spectral parameters as percent error (type I analysis with $k = 1$). In general, we found the parameter sets to be over determined in that the parameters of individual lineshape functions were highly correlated. For example, in $\epsilon''_j(\omega)$ fits to benzene data using the L−CI−G basis, α_j and ω_j of the CI function (eq 14) show a correlation of 0.98, whereas ω_j and σ_j of the Gaussian show a correlation of 0.94. Correlations between the parameters of distinct line-shape functions were small or absent. In bases with a larger number of terms, such as the all-L basis, the correlation between the width and frequency parameters increases. The implications of parameter correlations in the basis sets are discussed below.

Results

The THz-TDS and OHD-RIKES data analyzed in this report were collected at temperatures separated by ≤ 3 °C. Although temperature can affect the experimental data directly through changes in relaxational rate constants and indirectly by changes in intermolecular forces through the density, such effects are small for this temperature difference[18,19] and insignificant to our evaluation of the correspondence between the extracted spectra.

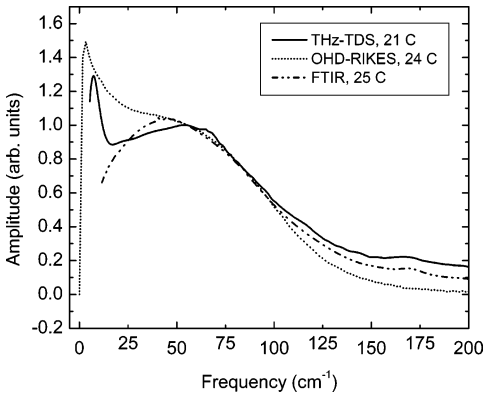

Figure 3. Comparison of the experimental benzene spectra. The spectra have been normalized to the amplitude at 55 cm^{-1} in each curve.

Dynamical Constants. One of the significant benefits of the OHD-RIKES technique is direct access to the temporal response function of a material; when the time constants of the response components are well separated they can be determined with high precision.[35] The orientational diffusion components of the OHD-RIKES response satisfy this criterion and can be used to objectively fix the $^1/_e$ lifetime parameter(s) $[1/(\gamma_i - \beta_i)]$ of the Lorentzian function(s) (eqs 11 and 12) that will be used to fit the orientational diffusion contribution(s) to the THz-TDS and OHD-RIKES spectral densities. The agreement between the reorientational rate constants measured by OHD-RIKES and DLS is typically excellent,[36,37] and any discrepancies are critically investigated by exhaustive repetition of the OHD-RIKES measurement. At 24 °C, the diffusive reorientation of D_{6h} benzene is well described by a single exponential at times >3 ps, with $\tau_{\text{or}} = 2.55 \pm 0.15$ ps. This result has been reproducible over several years in separate laboratories[38] and independently verified by others.[39] We are unable to account for the discrepancy with the value $\tau_{\text{or}} \cong 3$ ps measured by DLS[5a] or by OHD-RIKES in another laboratory.[12] Unsymmetrical C_{2v} bromobenzene (at 23 °C) exhibits a more complicated biexponential relaxation at times >3 ps with $^1/_e$ times $\tau_{\text{or},1} = 10.9 \pm 0.2$ ps and $\tau_{\text{or},2} = 2.4 \pm 0.1$ ps, corresponding to diffusive reorientation about axes orthogonal and parallel to the Br substituent.[40] Toluene shows a single-exponential decay with $\tau_{\text{or}} = 4.80 \pm 0.05$ ps at 24 °C. By correspondence to bromobenzene and other monosubstituted benzenes, a biexponential decay due to multiaxis orientational diffusion might be expected in toluene; the absence of a second relaxation component is probably due to the relatively small difference in the inertial moments parallel and orthogonal to the ring substituent[28] and the approximate equality of the corresponding reorientational rate constants.

Spectral Analyses. In Figure 3, our THz-TDS and OHD-RIKES spectra for benzene are plotted with a recent FTIR spectrum.[41] The THz-TDS data shows excellent qualitative agreement with the FTIR spectrum, replicating the prominent 60 cm^{-1} band as well as the diagnostic feature at $\sim$170 cm^{-1}. Both FIR spectra exhibit higher amplitude at frequencies >100 cm^{-1} than the OHD-RIKES spectrum. We expect agreement between the THz-TDS and FTIR spectra; the higher amplitude of the THz-TDS spectrum at frequencies >140 cm^{-1} and the

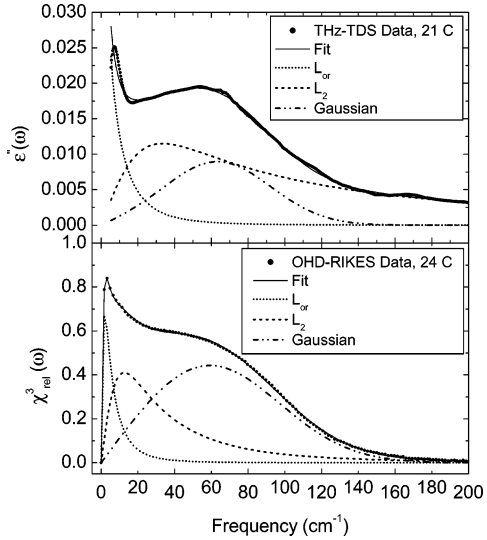

Figure 4. Fits to $\epsilon''(\omega)$ and $\chi^{(3)}_{rel}(\omega)$ spectra of benzene at 21 and 24 °C, respectively. See Table 1 for the parameters of the fitted components.

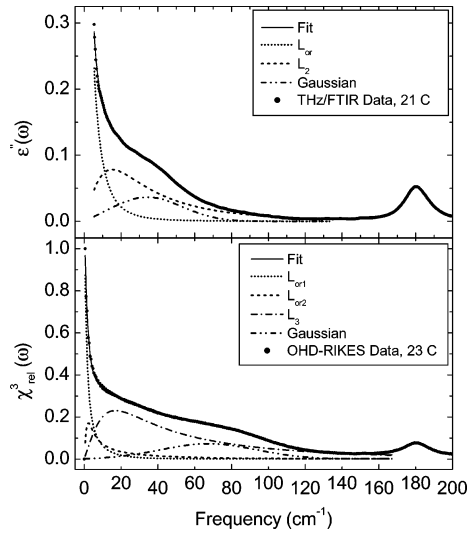

Figure 5. Fits to $\epsilon''(\omega)$ and $\chi^{(3)}_{rel}(\omega)$ spectra of bromobenzene at 21 and 23 °C, respectively. See Table 2 for the parameters of the fitted components.

absence of the orientational diffusion contribution in the FTIR spectrum at low frequency are under investigation.

Figures 4, 5, and 6 graphically display the modal decomposition of $\epsilon''_j(\omega)$ and $\chi^{(3)}_{eff}(\omega)$ for benzene, bromobenzene, and toluene using the L−L−G mode basis, the fitted parameters of which are listed in Tables 1−3. The $\epsilon''_j(\omega)$ and $\chi^{(3)}_{eff}(\omega)$ of all three liquids are well fit with a single Lorentzian (L_{or}) used to describe the reorientational diffusion. We note, however, that an additional Lorentzian is warranted to account for a second apparent orientational diffusion coordinate in the OHD-RIKES data of bromobenzene (vide supra). When two Lorentzians (L_{or1}, L_{or2}) were used (with the $1/(\gamma_i - \beta_i)$ the lineshape parameters constrained to reproduce the 10.9 and 2.4 ps $^1/_e$ times from the OHD-RIKES data), we found no improvement to the $\epsilon''_j(\omega)$ fit and only marginal improvement to the $\chi^{(3)}_{eff}(\omega)$ fit. Conversely, when a single orientational Lorentzian is used and the constraint pinning the value $1/(\gamma_i - \beta_i)$ to the τ_{or} lifetime measured by OHD-RIKES is relaxed, good fits are also obtained where $1/(\gamma_i - \beta_i) = 7.2$ and 4.8 ps in $\epsilon''_j(\omega)$ and $\chi^{(3)}_{eff}(\omega)$, respectively, which are intermediate to the 10.9 and 2.4 ps OHD-RIKES $^1/_e$ times. The fit to $\chi^{(3)}_{eff}(\omega)$ is slightly improved at frequencies ≤ 20 cm^{-1} in the $L_{or1}-L_{or2}-L-G$ basis, and we focus our discussion on that parametrization to ensure consistency between

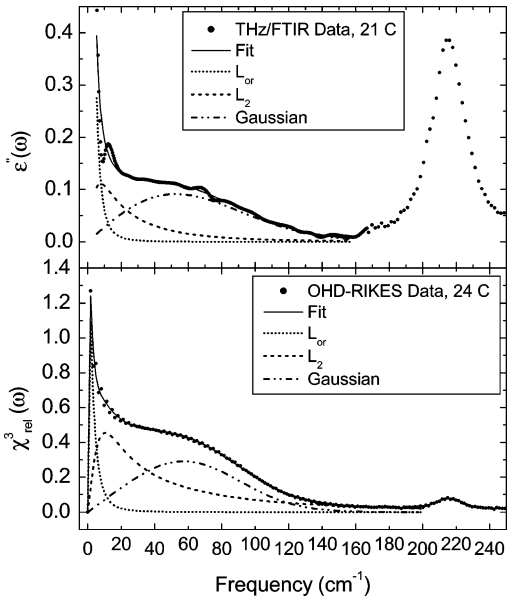

Figure 6. Fits to $\epsilon''(\omega)$ and $\chi^{(3)}_{rel}(\omega)$ spectra of toluene at 21 and 24 °C, respectively. See Table 3 for the parameters of the fitted components.

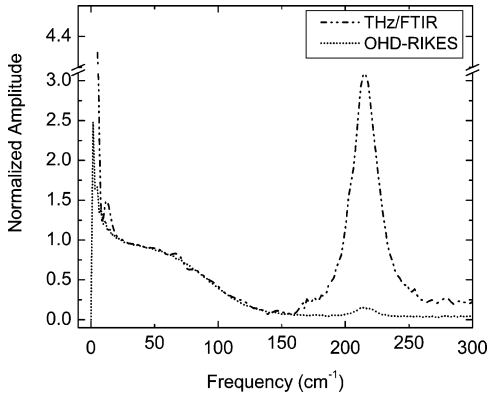

Figure 7. $\epsilon''(\omega)$ and $\chi^{(3)}_{rel}(\omega)$ spectra of toluene from Figure 6 normalized to amplitude at 24 cm^{-1} and overlaid for comparison.

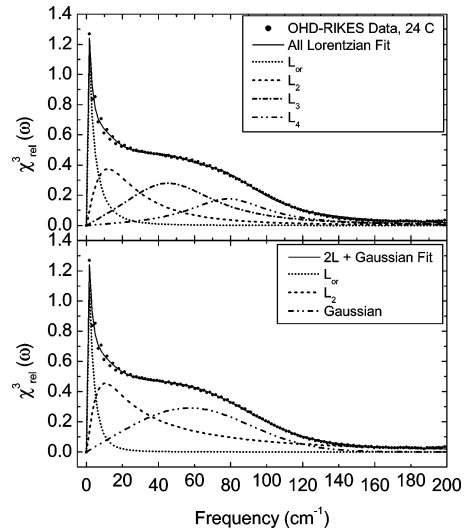

Figure 8. Comparison of fits to (i) a mixed basis (2 Lorentzians plus Gaussian, bottom panel) and (ii) an all-Lorentzian combination (top panel) for OHD-RIKES data of toluene.

TABLE 1: Benzene Data[a]

L-L-G Basis Best-Fit Parameters							
THz osc. type	A (%)	$\bar{\nu}_j$ (cm^{-1})	$\bar{\sigma}_j$, $\bar{\gamma}'$, or α (cm^{-1})	RIKES osc. type	A (%)	$\bar{\nu}_j$ (cm^{-1})	$\bar{\sigma}_j$, $\bar{\gamma}'$, or α (cm^{-1})
L_{or}	10.	7.34 (0.02)	14.02 (0.06)	L_{or}	9.0	5.94 (0.01)	9.539 (0.03)
L_2	63.4	124.74 (0.85)	246.9 (0.22)	L_2	29.8	31.25 (0.33)	43.31 (0.12)
G	26.6	63.2 (0.07)	56.9 (0.1)	G	56.7	57.99 (0.04)	76.31 (0.03)

L_{or} time constant	THz (ps)	RIKES (ps)
decay	2.55 (0.48)	2.55 (0.17)
rise	0.22 (0.07)	0.3 (0.04)

L-CI-G Basis Best-Fit Parameters							
THz osc. type	A (%)	$\bar{\nu}_j$ (cm^{-1})	$\bar{\sigma}_j$, $\bar{\gamma}'$, or α (cm^{-1})	RIKES osc. type	A (%)	$\bar{\nu}_j$ (cm^{-1})	$\bar{\sigma}_j$, $\bar{\gamma}'$, or α (cm^{-1})
L_{or}	16.2	12.25 (43)	37.16 (45)	L_{or}	15.6	17.4 (0.15)	73.75 (0.3)
CI	42.6	115 (1)	0.6 (27)	CI	19.9	15.74 (0.4)	0.62 (24)
G	41.2	53.7 (0.2)	69.3 (0.2)	G	64.5	57.5 (0.1)	77.1 (0.1)

L_{or} time constant	THz (ps)	RIKES (ps)
decay	2.55 (1000)	2.55 (12)
rise	0.075 (50)	0.037 (0.3)

All-L Basis Best-Fit Parameters							
THz osc. type	A (%)	$\bar{\nu}_j$ (cm^{-1})	$\bar{\sigma}_j$, $\bar{\gamma}'$, or α (cm^{-1})	RIKES osc. type	A (%)	$\bar{\nu}_j$ (cm^{-1})	$\bar{\sigma}_j$, $\bar{\gamma}'$, or α (cm^{-1})
L_{or}	0	7.36 (large)	14.05 (large)	L_{or}	12.3	8.17 (0.2)	17.1 (0.1)
L_2	24.7	235 (large)	874 (large)	L_2	15.6	96.2 (0.04)	21.0 (0.23)
L_3	45.0	71.58 (2)	40.75 (5)	L_3	23.5	70.9 (0.1)	21.6 (0.7)
L_4	30.3	121 (large)	1766 (large)	L_4	27.4	46.8 (0.3)	24.5 (1.3)
L_5				L_5	21.2	23.4 (50)	24.5 (50)

L_{or} time constant	THz (ps)	RIKES (ps)
decay	2.55 (large)	2.55 (1.9)
rise	0.22 (large)	0.18 (0.16)

[a] The frequency ($\bar{\nu}$), Lorentzian width ($\bar{\gamma}'$), and Gaussian width ($\bar{\sigma}$) parameters are given in wavenumber and are related to linear frequency by $\upsilon = c\bar{\nu}$ and $\gamma' = c\bar{\gamma}'$ where c is the speed of light. The parameter A is the normalized areal contribution of the term, α is the frequency exponent in the CI function (where used), and the numbers in parentheses are the fitting standard deviation in percent. In the L-L-G basis, the RIKES L_2 is "overdamped" with $\tau_{1/e} \approx 400$ fs, $\tau_{rise} \approx 90$ fs, the THz L_2 is overdamped with $\tau_{1/e} \approx 157$ fs, and $\tau_{rise} \approx 12$ fs. The L_{or} time constants (for the orientational diffusion contribution) are calculated from the functional parameters as described in the text.

the time and frequency domain representations of the OHD-RIKES bromobenzene data.

The Gaussian contributions to $\chi^{(3)}_{eff}(\omega)$ have center frequencies near 57 cm^{-1} in benzene and toluene, and ~68 cm^{-1} in bromobenzene, with width parameters in the range 51 to 80 cm^{-1}. The $\epsilon''_j(\omega)$ and $\chi^{(3)}_{eff}(\omega)$ fits for toluene correspond well when compared term-for-term (Table 3, cases i and ii), the principal difference being a slightly larger contribution to $\epsilon''_j(\omega)$ from the intermediate Lorentzian. The basis of this correspondence is shown in Figure 7, where the spectra are normalized at 24 cm^{-1} and overlaid. In contrast, $\epsilon''_j(\omega)$ of benzene requires a significantly distinct center frequency for the intermediate Lorentzian (~125 cm^{-1}) compared to that of the $\chi^{(3)}_{eff}(\omega)$ fit (~31 cm^{-1}) to account for the increased amplitude of $\epsilon''_j(\omega)$ at high frequency ($\geq$100 cm^{-1}), whereas the Gaussian terms are similar with frequencies of 63 and 58 cm^{-1}, respectively (Table 1). In bromobenzene, $\epsilon''_j(\omega)$ is significantly red shifted from $\chi^{(3)}_{eff}(\omega)$; the Gaussian term in $\epsilon''_j(\omega)$ is ~30 cm^{-1} lower than the corresponding fitted term in $\chi^{(3)}_{eff}(\omega)$ (Table 2, case ii)). This spectral "shift" is most likely traceable to the different selection rules for THz-TDS and OHD-RIKES and to a large difference in magnitude between the permanent dipole moment along the Br axis (1.70 D) and the induced dipole moment along the orthogonal axis in the molecular plane. In $\chi^{(3)}_{eff}(\omega)$, librations about both axes are Raman active with commensurable cross section, whereas in $\epsilon''_j(\omega)$, the much smaller cross section of the higher-frequency libration results in its apparent absence from the spectrum.

The fitted parameters for the bases L−CI−G and all-L are presented in Tables 1−3. Only the L−CI−G basis gave high-quality three-term fits that were typically as good as those in the L−L−G basis. The differences noted between $\epsilon''_j(\omega)$ and $\chi^{(3)}_{eff}(\omega)$ of benzene and bromobenzene in the L−L−G basis are largely corroborated in the L−CI−G and all-L fits. The all-L basis required 5, 4, and 4 terms to generate fits of comparable but typically lesser quality in benzene, bromobenzene, and toluene, respectively. In Figure 8, we compare the fits to $\chi^{(3)}_{eff}(\omega)$ of toluene in the L−L−G and all-L bases. In addition to requiring a 4th term, the all-L basis does not match the high-frequency band edge at frequencies >80 cm^{-1} as well as bases using a Gaussian. The all-L fits to $\chi^{(3)}_{eff}(\omega)$ of benzene and bromobenzene were similarly unable to match the data at high frequency. Our fits to $\chi^{(3)}_{eff}(\omega)$ of benzene and bromobenzene in the L−CI−G basis substantially agree with a previous multimode spectral decomposition in a stimulated Raman gain spectroscopy[42] (SRG) study. In the SRG study, $\nu_{CI} = 8.3$ cm^{-1} (with a CI frequency exponent $\alpha = 0.57$), $\nu_G = 52$ cm^{-1}, and $\sigma_G = 42$ cm^{-1} for benzene. We determined these parameters to be $\nu_{CI} = 9.8$ cm^{-1}, $\nu_G = 57.5$ cm^{-1}, and $\sigma_G = 77$ cm^{-1} (Table 1). For bromobenzene, the SRG study gave $\nu_{CI} = 7$ cm^{-1}, $\nu_G = 30$ cm^{-1}, and $\sigma_G = 47$ cm^{-1}. In a three-term fit (one term for orientational diffusion, vide supra) we determined these

TABLE 2: Bromobenzene Data[a]

L-L-G Basis Best-Fit Parameters

(i)sum of two Lorentzians (L) plus a Gaussian (G)
RIKES data L_2 is overdamped with $\tau_{1/e} \approx 667$ fs, $\tau_{rise} \approx 20$ fs,
the THz L_2 is overdamped with $\tau_{1/e} \approx 314$ fs, $\tau_{rise} \approx 115$ fs

THz osc. type	*A* (%)	$\bar{\nu}_j$ (cm^{-1})	$\bar{\sigma}_j$, $\bar{\gamma}'$, or α (cm^{-1})	RIKES osc. type	*A* (%)	$\bar{\nu}_j$ (cm^{-1})	$\bar{\sigma}_j$, $\bar{\gamma}'$, or α (cm^{-1})
L_{or}	21.8	1.47 (0.01)	6.69 (0.03)	L_{or}	19.4	6.00 (0.15)	37.25 (0.29)
L_2	54.1	32.65 (0.001)	40.03 (0.42)	L_2	42.2	46.33 (6.98)	139.1 (13.5)
G	24.1	34.239 (0.35)	37.15 (0.34)	G	38.7	42.5 (5.3)	80.1 (2.6)

L_{or} time constant	THz (ps)	RIKES (ps)
decay	32.445 (1.3)	10.9 (24)
rise	0.41 (0.03)	0.07 (0.3)

(ii)sum of three Lorentzians (L) plus a Gaussian (G)
RIKES L_3 is overdamped with $\tau_{1/e} \approx 190$ fs, $\tau_{rise} \approx 58$ fs,
the THz L_3 is overdamped with $\tau_{1/e} \approx 265$ fs, $\tau_{rise} \approx 165$ fs

THz osc. type	*A* (%)	$\bar{\nu}_j$ (cm^{-1})	$\bar{\sigma}_j$, $\bar{\gamma}'$, or α (cm^{-1})	RIKES osc. type	*A* (%)	$\bar{\nu}_j$ (cm^{-1})	$\bar{\sigma}_j$, $\bar{\gamma}'$, or α (cm^{-1})
L_{or1}	20.85	1.46 (0.01)	6.64 (0.03)	L_{or1}	5.25	2.86 (0.15)	8.66 (0.29)
L_{or2}	2.81	10.62 (5)	26.62 (12)	L_{or2}	24.5	12.7 (1.0)	37.6 (5.8)
L_3	60.41	32.25 (5.)	36.01 (10)	L_3	55.7	57.7 (8)	73.6 (15)
G	15.93	38.9 (0.35)	30.93 (0.34)	G	14.86	67.53 (5.3)	50.88 (2.6)

orientational time constants	THz (ps)	RIKES (ps)
L_{or1} decay	32.64 (1.3)	10.9 (6.1)
rise	0.41 (0.03)	0.325 (0.3)
L_{or2} decay	2.4 (170)	2.4 (100)
rise	0.11 (13)	0.08 (6.5)

L-CI-G Basis Best-Fit Parameters

(i) sum of a Lorentzian, a CI term, and a Gaussian

THz osc. type	*A* (%)	$\bar{\nu}_j$ (cm^{-1})	$\bar{\sigma}_j$, $\bar{\gamma}'$, or α (cm^{-1})	RIKES osc. type	*A* (%)	$\bar{\nu}_j$ (cm^{-1})	$\bar{\sigma}_j$, $\bar{\gamma}'$, or α (cm^{-1})
L_{or}	13.9	1.16 (5)	4.24 (10)	L_{or}	11.1	2.37 (0.1)	6.04 (0.5)
CI	81.8	21.92 (0.2)	0.6	CI	32.1	14.3 (1)	0.6 (20)
G	4.3	41.04 (0.1)	17.7 (0.2)	G	56.8	38.9 (2)	96.1 (0.5)

L_{or} time constant	THz (ps)	RIKES (ps)
decay	32.8 (300)	10.9 (7)
rise	0.65 (10)	0.48 (0.55)

(ii) sum of two Lorentzians, a CI term, and a Gaussian

THz osc. type	*A* (%)	$\bar{\nu}_j$ (cm^{-1})	$\bar{\sigma}_j$, $\bar{\gamma}'$, or α (cm^{-1})	RIKES osc. type	*A* (%)	$\bar{\nu}_j$ (cm^{-1})	$\bar{\sigma}_j$, $\bar{\gamma}'$, or α (cm^{-1})
L_{or1}	4.26	0.464 (1)	0.743 (1)	L_{or1}	13.66	3.92 (0.1)	16.1 (0.2)
L_{or2}	17.25	7.422 (0.9)	13.56 (1)	L_{or2}	6.23	8.48 (0.1)	17.4 (0.2)
CI	71.85	22.9 (0.2)	0.6	CI	74.05	32.3 (0.1)	0.6 (4)
G	6.63	39.81 (0.1)	21.04 (0.2)	G	6.06	78.97 (0.1)	32.1 (0.2)

orientational time constants	THz (ps)	RIKES (ps)
L_{or1} decay	33.1 (8)	10.9 (7.5)
rise	4.57 (1.5)	0.17 (0.2)
L_{or2} decay	2.4 (10)	2.4 (2)
rise	0.234 (1.3)	0.175 (0.24)

All-L Basis Best-Fit Parameters

THz osc. type	*A* (%)	$\bar{\nu}_j$ (cm^{-1})	$\bar{\sigma}_j$, $\bar{\gamma}'$, or α (cm^{-1})	RIKES osc. type	*A* (%)	$\bar{\nu}_j$ (cm^{-1})	$\bar{\sigma}_j$, $\bar{\gamma}'$, or α (cm^{-1})
L_{or1}	10.1	1.46 (0.2)	6.64 (0.6)	L_{or1}	11.6	2.86 (0.1)	8.06 (0.2)
L_{or2}	30.0	10.6 (0.2)	26.6 (0.4)	L_{or2}	11.0	12.7 (0.05)	37.7 (0.1)
L_3	20.0	44.8 (0.1)	18.8 (0.2)	L_3	50.6	39.1 (10)	49.5 (20)
L_4	39.9	30.7 (0.1)	26.9 (0.1)	L_4	26.8	75.9 (1)	34.1 (1.5)

orientational time constants	THz (ps)	RIKES (ps)
L_{or1} decay	33.1 (26)	10.1 (3.7)
rise	0.41 (0.6)	0.35 (0.2)
L_{or2} decay	2.4 (6)	2.4 (2)
rise	0.1 (0.4)	0.075 (0.5)

[a] The parameters are the same as those in Table 1.

TABLE 3: Toluene Data[a]

L-L-G Basis Best-Fit Parameters

(i) L_{or} are constrained to replicate the OHD-RIKES τ_{or}, RIKES L_2 is overdamped with $\tau_{1/e} \approx 505$ fs, $\tau_{rise} \approx 34$ fs, THz L_2 is overdamped with $\tau_{1/e} \approx 274$ fs, $\tau_{rise} \approx 56$ fs

THz osc. type	A (%)	$\bar{\nu}_j$ (cm^{-1})	$\bar{\sigma}_j$, $\bar{\gamma}'$, or α (cm^{-1})	RIKES osc. type	A (%)	$\bar{\nu}_j$ (cm^{-1})	$\bar{\sigma}_j$, $\bar{\gamma}'$, or α (cm^{-1})
L_{or}	12.0	2.34 (185)	3.02 (301)	L_{or}	9.7	3.07 (0.1)	4.82 (0.2)
L_2	59.2	46.98 (0.19)	66.72 (0.32)	L_2	46.7	41.87(2.2)	88.82 (0.31)
G	28.8	67.38 (0.14)	54.21 (0.30)	G	43.6	56.85 (0.15)	66.43 (0.17)

L_{or} time constant	THz (ps)	RIKES (ps)
decay	4.78 (500)	4.8 (1.1)
rise	1.39 (263)	0.71 (0.27)

(ii) THz L_{or} is adjusted for the rank of the dipolar time-correlation function (see text)

THz osc. type	A (%)	$\bar{\nu}_j$ (cm^{-1})	$\bar{\sigma}_j$, $\bar{\gamma}'$, or α (cm^{-1})	RIKES osc. type	A (%)	$\bar{\nu}_j$ (cm^{-1})	$\bar{\sigma}_j$, $\bar{\gamma}'$, or α (cm^{-1})
L_{or}	12.0	1.74 (103)	4.304 (400)	L_{or}	9.7	3.07 (0.1)	4.82 (0.2)
L_2	59.2	43.88 (0.18)	64.93 (0.27)	L_2	46.7	41.87 (2.2)	88.82 (0.31)
G	28.8	66.33 (0.11)	56.74 (0.23)	G	43.6	56.85 (0.15)	66.43 (0.17)

L_{or} time constant	THz (ps)	RIKES (ps)
decay	14.44 (2000)	4.8 (1.1)
rise	0.67 (437)	0.71 (0.3)

L-CI-G Basis Best-Fit Parameters

THz osc. type	A (%)	$\bar{\nu}_j$ (cm^{-1})	$\bar{\sigma}_j$, $\bar{\gamma}'$, or α (cm^{-1})	RIKES osc. type	A (%)	$\bar{\nu}_j$ (cm^{-1})	$\bar{\sigma}_j$, $\bar{\gamma}'$, or α (cm^{-1})
L_{or}	9.9	1.79 (15)	2.0 (5)	L_{or}	16.23	5.27 (0.1)	13.1 (0.25)
CI	73.88	35.72 (0.3)	0.6 (10)	CI	63.75	36.88 (0.2)	0.6 (50)
G	16.23	73.04 (0.1)	48.6 (0.3)	G	20.03	68.19(0.2)	52.09 (0.2)

L_{or} time constant	THz (ps)	RIKES (ps)
decay	4.8 (50)	4.8 (3.5)
rise	2.97 (32)	0.22 (0.3)

All-L Basis Best-Fit Parameters

THz osc. type	A (%)	$\bar{\nu}_j$ (cm^{-1})	$\bar{\sigma}_j$, $\bar{\gamma}'$, or α (cm^{-1})	RIKES osc. type	A (%)	$\bar{\nu}_j$ (cm^{-1})	$\bar{\sigma}_j$, $\bar{\gamma}'$, or α (cm^{-1})
L_{or}	10.9	1.98 (5)	2.33 (10)	L_{or}	12.0	4.23 (0.1)	8.6 (0.3)
L_2	25.9	22.9 (0.1)	17.65 (0.5)	L_2	22.3	83.0 (0.11)	27.2 (0.8)
L_3	63.42	70.0 (0.1)	41.4 (0.1)	L_3	28.2	25.6 (4)	31.3 (7)
L_4				L_4	36.4	55.1 (0.6)	33.4 (2.4)

L_{or} time constant	THz (ps)	RIKES (ps)
decay	4.8 (31)	4.8 (2.7)
rise	2.16 (20)	0.35 (0.35)

[a] The parameters are the same as those in Table 1.

parameters to be $\nu_{B-L} = 8.6$ cm^{-1}, $\nu_G = 39$ cm^{-1}, and $\sigma_G = 96$ cm^{-1} (Table 2). In both liquids, the Lorentzian term for orientational diffusion was essentially identical in the OHD-RIKES and SRG fits. The differences between the SRG and our OHD-RIKES fits reside primarily in the width parameters of the Gaussian term and may be traceable to the assumption in the SRG study of a single intrinsic frequency parameter for the orientational Lorentzian and the Gaussian terms.[42]

Discussion

As noted in the Introduction, Rønne et al.[18] measured the spectral densities of benzene and toluene by THz-TDS and OHD-RIKES as a function of temperature in the range of −7 to 75 °C. There are two noteworthy distinctions to be made between that report and the work presented here: the frequency range of our THz-TDS spectrometer is slightly wider at both the low and high end of the range, and our treatment of the OHD-RIKES data is different. The frequency range of our THz-TDS measurements is ∼5 to 140 cm^{-1} compared to the ∼7 to 110 cm^{-1} range previously reported.[18] The practical distinction is that we clearly discern the tail of the contribution by orientational diffusion to the THz-TDS spectra at low frequency in all three liquids at 21 °C (top panels of Figures 4, 5, and 6), whereas this contribution was previously seen only in toluene.[18] Second, in comparing the THz-TDS and OHD-RIKES spectra of benzene, Rønne et al. modified the OHD-RIKES spectra by subtraction of response components deemed traceable to orientational diffusion[12] (Appendix). This modification reduces the amplitude of the OHD-RIKES spectral density function (deduced via eq 10) in the frequency range of 0 to ∼70 cm^{-1} where the observed differences between the THz-TDS and OHD-RIKES spectra were traced to a specific physical model of intermolecular interactions.[18,19] Because our THz-TDS data show contributions from diffusive reorientation, the corresponding components in the experimental OHD-RIKES data were retained to ensure equivalent starting points for the modal decompositions of $\epsilon''_j(\omega)$ and $\chi^{(3)}_{eff}(\omega)$.

Two important distinctions between the OHD-RIKES and THz-TDS techniques are (1) in THz-TDS, the matter−field coupling is via the permanent dipole moment, whereas in OHD-RIKES, the coupling is via the polarizability anisotropy, and (2) the rank l of the time-correlation function (TCF) for these properties is $l = 1$ and $l = 2$, respectively. The difference in rank implies a scaling factor of 3X for the $^1/_e$ lifetimes of first-order contributions to the dipole TCF (measured by THz-TDS) relative to the corresponding decay process in the polarizability TCF (measured by OHD-RIKES).[1,18,20] For example, the orientational diffusion components of the polarizability TCF of bromobenzene are $\tau_{or,1} = 10.9$ ps and $\tau_{or,2} = 2.4$ ps for motion about axes perpendicular and parallel to the Br substituent (and in the molecular plane). In THz-TDS, it is therefore expected that $\tau_{or,1} \cong 32.7$ ps because the corresponding coordinate possesses a large permanent dipole moment that interacts with the interrogating THz waveform via the dipolar TCF of rank $l = 1$. Although the fits to $\epsilon''_j(\omega)$ of bromobenzene were substantially insensitive to the value of $1/(\gamma_i - \beta_i)$ (and τ_{or}), the constraint of replicating the 32.7 ps value was retained for consistency. Conversely, the rank of the TCF for interaction-induced dipole moments is determined by the operative term in the multipole expansion; the TCF of a quadrupole-induced dipole moment has the rank $l = 2$, and the dynamics of such coordinates will be the same in either THz-TDS or OHD-RIKES.[18] For systems with both permanent and multipole-induced dipole moments, the dipole TCF could be a superposition of terms varying in rank and optical cross section and could pose a complication to the analysis and interpretation of the data. This may be particularly relevant for toluene, where the relatively small dipole moment along the axis of the methyl substituent (0.36 D) may be of similar magnitude as the quadrupole-induced dipole along the orthogonal axis in the plane. (We note that a corresponding situation may exist in bromobenzene, with a much larger difference between the permanent and quadrupole-induced dipole moments.) Therefore, we tested the fits to $\epsilon''_j(\omega)$ of toluene by setting the constraint on $1/(\gamma_i - \beta_i)$ of the lowest frequency Lorentzian to either 4.8 (TCF rank $l = 2$) or 14.4 ps (TCF rank $l = 1$) and found that only the parameters of the constrained term were affected. The general stability of the L_{or} fit parameters were tested for all three liquids, all by relaxing the τ_{or} constraint on $1/(\gamma_i - \beta_i)$ and rerunning the fitting routine while holding fixed the previously optimized parameters of the remaining terms (e.g., L_2 and G of the L−L−G basis). Under those conditions, the L_{or} fit parameters were stable. If the constraint was relaxed and the parameters of the remaining terms allowed to float, then the optimized L_{or} parameters typically gave $1/(\gamma_i - \beta_i)$ in the range of $1.5\tau_{or}$ to $0.5\tau_{or}$, with small variations in the frequency and width parameters of the other terms.

When either the number or functional form of terms in some of the fitting combinations is varied, the values of the frequency, width, and areal parameters change. For example, when the three-term $L_{or}-L_2-G$ fit to $\chi^{(3)}_{eff}(\omega)$ of bromobenzene is altered by the addition of the second orientational diffusion term (to account for the 2.4-ps relaxation component with an $L_{or1}-L_{or2}-L_3-G$ function set), the frequency of the 3rd Lorentzian shifts from 46 to 58 cm^{-1} and its area increases from 42 to 56%, whereas the Gaussian frequency shifts from 42 to 68 cm^{-1} and the area decreases from 39 to 15%. Similarly, when the highest frequency Gaussian of the 4-term $\chi^{(3)}_{eff}(\omega)$ fit of bromobenzene is replaced with a Lorentzian ($L_{or1}-L_{or2}-L_3-L_4$ function set), the area of the 3rd Lorentzian changes from 56 to 51% and the frequency shifts from 58 to 39 cm^{-1}. Concomitantly, the 4th Lorentzian acquires an area of 26% and frequency of 76 cm^{-1} (whereas the Gaussian area was 15% with a frequency of 68 cm^{-1}). In these examples, when the frequency parameter increased, the width parameter decreased such that the shape and position of the functional term in the spectrum were generally retained. Such differences are attributed to the distinct shapes of the CI, Lorentzian, and Gaussian functions at intermediate and high frequencies. These parameter shifts place limits on the uniqueness of the fits, particularly when a correlation is imposed, as in the L_{or} terms where the parameters $1/(\gamma_i - \beta_i)$ are set equal to τ_{or} that was determined from the OHD-RIKES data. We have noted that the inclusion of two terms for orientational diffusion coordinates in bromobenzene results in a significant shift in the fitted Gaussian to higher frequency and lower width (Table 2) for a small improvement in the fit to the $\chi^{(3)}_{eff}(\omega)$ spectral density. However, the larger basis for $\chi^{(3)}_{eff}(\omega)$ should be regarded as physically validated by the observation of two first-order decay components in the time-domain OHD-RIKES data. In contrast, the fit to $\epsilon''_j(\omega)$ of bromobenzene (with $\tau_{or} = 32.4$ ps) is neither noticeably improved nor are the high-frequency L terms significantly shifted by the inclusion of the second orientational diffusion Lorentzian (Table 2, cases i and ii). In this regard, we reiterate that our primary objective in these "modal" decompositions is to generate parametrizations that permit a comparison of the experimental spectra, not to trace portions of the measured spectra to specific structures or interactions that we cannot presently validate. A physically validated modal decomposition may well have a larger number of terms than our minimum bases; for the analysis presented here, only the orientational diffusion terms (the lowest-frequency Lorentzians) are well validated. Conversely, the spectra of libration and collision-induced phenomena are the objects of ongoing theoretical and experimental work.

Our results generally support the proposal of Rønne et al.,[18] that the information content of the dipolar and polarizability correlation functions is different and may be exploited to investigate and characterize distinct types of intermolecular interactions via complementary THz-TDS and OHD-RIKES studies. The benzene spectra in Figure 4 and the fitting results in Table 1 additionally support their conclusion that the $\epsilon''_j(\omega)$ spectrum of benzene is significantly different than that of $\chi^{(3)}_{eff}(\omega)$ in the 0.4−1.8 THz (13−60 cm^{-1}) range, despite the discrepancy in our respective treatment of the OHD-RIKES data. Additionally, the deviation between the $\epsilon''_j(\omega)$ data and the fit in the 0.2−0.6 THz (7−20 cm^{-1}) range (Figure 4, top) suggests that orientational diffusion in the dipolar TCF of benzene is more complex than in the polarizability TCF ($\chi^{(3)}_{eff}(\omega)$). Following the suggestion of Rønne et al.[18] concerning the differential sensitivity of OHD-RIKES and THz-TDS to the in-plane libration of the quadrupole-induced dipole, it is reasonable to anticipate that both the in-plane and out-of-plane diffusive motions of the induced dipole will be observed by THz-TDS, whereas OHD-RIKES will witness only the out-of-plane motion. Thus, contributions to $\epsilon''_j(\omega)$ from two diffusion coordinates with similar but not identical dynamical constants could account for the inability of a single lineshape term to fit the benzene data precisely at low frequencies.

Conversely, our results contrast with a recently reported Brownian oscillator spectral decomposition,[20] where fits of FIR and OHD-RIKES spectra required up to two additional terms (six parameters) to fit the same spectral range, and the $\epsilon''_j(\omega)$ and $\chi^{(3)}_{eff}(\omega)$of several liquids could be related by differentially rescaling the amplitudes of a set of modes with fixed frequency

and width parameters. Only in liquid toluene are we able to rescale the amplitude parameters at fixed modal bandwidths and frequencies to obtain a reasonable fit to both $\epsilon''_j(\omega)$ and $\chi^{(3)}_{\text{eff}}(\omega)$. In benzene and bromobenzene, we find that the $\epsilon''_j(\omega)$ and $\chi^{(3)}_{\text{eff}}(\omega)$ cannot be reconciled in this way because the pronounced differences in the measured spectra do not support modal decomposition to a shared basis. A further distinction with the Brownian oscillator analysis is that we do not attempt to "couple" the modes in a directional cascade by pinning the decay of high-frequency vibrational coordinates to the rise-time(s) of lower-frequency diffusion coordinates.[20] Such coupling excludes the possibility of a superposition of librational and diffusive reorientational motions, thereby restricting orientational motion at any given time to either a zero rms displacement such as libration or a nonzero rms displacement such as reorientation. To the extent that local intermolecular interactions are approximately conservative, energy residing in the orientational motion about molecule-fixed axes will be constant; what the motion will be called depends on the local details of a stochastic potential. For those molecules in sharply curved potentials with large barriers, rms reorientation to a new mean position is prohibited and the motion is librational; for those in a relatively flat potential with low barriers, net reorientation is allowed. It is not difficult to envision a superposition of distinct distributions of molecules in instantaneous potentials with specific motional constraints, or molecules in a "random walk" among fluctuations in the potential curvature such that instances of librational and reorientational motion are superposed or interleaved. In the molecule frame of reference, motional characteristics reflect the instantaneous conditions of constraint. By this argument, we do not propose that local molecular motions are rigorously conservative and that mechanical energy does not dissipate via coupling to a "continuum" bath. Rather, we suggest that the superposition of dynamical states to represent molecular dynamics should not be constrained by an artificial causality, which states that low-frequency modes cannot be populated by high-bandwidth excitation except via the decay of higher-frequency modes.

The final distinctions between this report and the Brownian oscillator analysis[20] are the premises of the latter that neither nonlinear mode coupling nor inhomogeneous broadening are operative in the Raman ($\chi^{(3)}_{\text{eff}}(\omega)$) or dipolar ($\epsilon''_j(\omega)$) vibrational dynamics. The former premise contrasts with the invocation by Rønne et al. of three-body effects[18,19] to explain the distinct temperature dependence of the THz-TDS and OHD-RIKES spectral densities. The latter premise appears to neglect novel attributes of vibrational coordinates in the experimental frequency range,[14] as well as the convergence of the fit Brownian oscillator bandwidth parameters to a common value for transitions equally separated in frequency;[20] a result that could be construed as evidence of inhomogeneous broadening. $\chi^{(3)}_{\text{eff}}(\omega)$ in the frequency range below $\sim$200 cm^{-1} is dominated by contributions arising from intermolecular vibrational coordinates defined by localized interactions of two or more molecules.[8,9,12] Intermolecular vibrational modes are distinguished from those of orientational or translational diffusion by the absence of the classical Debye−Stokes−Einstein temperature dependence and from intramolecular vibrational modes by their low frequency and extreme sensitivity to fluctuations in the local structure of the liquid, which dramatically modulate the intermolecular potential. In contrast, intermolecular fluctuations constitute small perturbations on the covalent potentials that define intramolecular vibrations; consequently, these modes are not expected to exhibit high sensitivity to intermolecular interactions.[43] These considerations suggest that conventional wisdom about line broadening of high-frequency intramolecular degrees of freedom does not apply directly to low-frequency intermolecular coordinates. The highest frequency motions in molecular liquids that result in rms displacements of intermolecular configurations and, hence, irreversible changes in the liquid structure and intermolecular potential are those of molecular orientation. The homogeneous line widths associated with orientational dynamics are typically on the order of a few wavenumbers, approximately an order of magnitude lower than either the mean frequency or the width of the bands in $\epsilon''_j(\omega)$ or $\chi^{(3)}_{\text{eff}}(\omega)$ and consequently are unable to account for the observed spectral width. Therefore, the concept of inhomogeneous broadening being responsible for the width of these spectra is neither unphysical nor unwarranted.

Despite our earlier caveat concerning physical interpretations of spectral decompositions, the parametrizations in Tables 1−3 can be conservatively interpreted to be decomposing the ultrafast molecular dynamics contributing to $\chi^{(3)}_{\text{eff}}(\omega)$ into diffusive orientational motions represented by the lowest-frequency Lorentzian and intermolecular librations represented by the Gaussian. The use of the Lorentzian to describe the spectra of diffusive degrees of freedom is well established in DLS[5] and FIR[23] spectroscopy. We have found that remarkable agreement with the OHD-RIKES temporal response is realized by a model for molecular libration that uses a single (inhomogeneous) Gaussian term in high-symmetry molecular liquids[14] and are investigating the ability of this model to describe $\chi^{(3)}_{\text{eff}}(\omega)$ in benzene and monosubstituted benzenes using only an overdamped Lorentzian for orientational diffusion plus a Gaussian for the intermolecular dynamics.[40] The interpretation of either the CI or intermediate frequency Lorentzian terms with respect to specific degrees of freedom is less clear. In the L−L−G basis, the intermediate-frequency Lorentzian can be regarded as a second homogeneously broadened oscillator or an intermediate-frequency inhomogeneous distribution function (the choice of a Gaussian distribution function to represent inhomogeneous broadening is neither unique nor required[11,34]). As a homogeneously broadened oscillator, the intermediate-frequency Lorentzian is overdamped in all three liquids, with $^1/_e$ times of 400, 670, and 500 fs for benzene, bromobenzene, and toluene, respectively. These time constants can be compared to those of the so-called "intermediate component" that underlies orientational relaxation in the time-domain OHD-RIKES response (Appendix). The OHD-RIKES time-domain response function for benzene shows $\tau_{\text{int}} = 450$ fs, for bromobenzene $\tau_{\text{int}} = 620$ fs, and for toluene $\tau_{\text{int}} = 790$ fs. Although the correspondence of the Lorentzian time constants to the experimental observations suggests a modal origin, attempts to unequivocally trace this response component to specific dynamical coordinates are currently unvalidated.[12,37,44] The mechanical coordinates identified from modal interpretations of the $\chi^{(3)}_{\text{eff}}(\omega)$ spectra should contribute to $\epsilon''_j(\omega)$, subject to the constraints of the dipole selection rule.[20] However, we do not anticipate a priori that the detailed spectral and temporal dependences of these mechanical coordinates on *n* body interactions and symmetry should be identical in the dipolar and polarizability probes. The interpretation of differences between the components of the $\epsilon''_j(\omega)$ and $\chi^{(3)}_{\text{eff}}(\omega)$ spectra is therefore speculative; although our results indicate that the spectra are distinct, the differences are unlikely to be traced to specific physical causes on the basis of information at a single point on the phase diagram of a material. To realize the full benefit of the complementary information available from THz-TDS and OHD-RIKES, the analysis of data

taken over a range of state parameters (such as T) and at the highest available experimental bandwidth will be required.

Conclusions

We have compared the dielectric loss ($\epsilon''_j(\omega)$) and Raman susceptibility ($\chi^{(3)}_{\text{eff}}(\omega)$) spectra of liquid benzene, bromobenzene, and toluene obtained via THz-TDS and OHD-RIKES, respectively, using a multimode spectral analysis where the measured spectra were fit to minimum combinations of Lorentzian, collision-induced, and Gaussian functions. The data and subsequent spectral analyses indicate that $\epsilon''_j(\omega)$ and $\chi^{(3)}_{\text{eff}}(\omega)$ cannot, in general, be decomposed to a shared set of mechanical coordinates with fixed frequencies and bandwidths. Both benzene and bromobenzene exhibit significant differences between $\epsilon''_j(\omega)$ and $\chi^{(3)}_{\text{eff}}(\omega)$, indicating that the dipolar and polarizability time-correlation functions are differentially sensitive to specific intermolecular interactions and that the information content of these spectra is not redundant. Our results support the general findings of Rønne et al.[18] in the benzene spectra at frequencies below 1.8 THz, but differ in that we clearly resolve the high-frequency wing of the orientational diffusion response in all three liquids. This and other discrepancies strongly suggest that the experiments of Rønne et al.[18] should be repeated with a larger THz frequency range and an expanded sample set; for example, in our data $\epsilon''_j(\omega)$ and $\chi^{(3)}_{\text{eff}}(\omega)$ of benzene diverge at frequencies >3.5 THz (~ 120 cm^{-1}), where the data of Rønne et al. stopped. Molecular dynamics simulations of liquid benzene that had been invoked to explain the distinct temperature dependence of $\epsilon''_j(\omega)$ and $\chi^{(3)}_{\text{eff}}(\omega)$ at low frequency also indicated that the difference would diminish at high frequency,[19] thus suggesting that a reexamination of the temperature effect over a larger THz bandwidth would be useful. Additionally, the strong correspondence observed in the $\epsilon''_j(\omega)$ of benzene and toluene by Rønne et al. suggests that $\epsilon''_j(\omega)$ and $\chi^{(3)}_{\text{eff}}(\omega)$ of toluene should differ where our result (at a single phase locus) shows that they are nearly identical (Figure 7 and Table 3). The pronounced differences in the bromobenzene spectra suggest that $\epsilon''_j(\omega)$ and $\chi^{(3)}_{\text{eff}}(\omega)$ in the monohalogenated benzenes may generally exhibit subtly distinct dependences on intermolecular interactions and state variables as well as differences traceable to the Raman and dipolar selections rules. Particularly interesting is the apparent lack of evidence in the $\epsilon''_j(\omega)$ of bromobenzene for the 2.4-ps reorientation and the ~ 67-cm^{-1} libration dynamics relative to $\chi^{(3)}_{\text{eff}}(\omega)$. We conclude that THz-TDS and OHD-RIKES generally offer complementary information about molecular and vibrational dynamics. However, detailed characterizations of intermolecular interactions and the assignment of spectral "fingerprints" will require the collection and analysis of spectra taken over ranges of state variables.

Appendix

In the OHD-RIKES data modification of Rønne et al.,[18] two contributions to the benzene OHD-RIKES response were identified with orientational diffusion in conformity with a previous analysis[12] and subtracted from the experimental data ($T(\tau)$, eq 8) prior to the extraction of the spectral density via the operations indicated in eq 10. We identify only one orientational contribution in the OHD-RIKES response of benzene. The origin of this disagreement can be traced to alternate interpretations of a universal characteristic of the OHD-RIKES response $R^{(3)}_{\text{eff}}(\tau)$ in nonassociated organic liquids; underlying the orientational diffusion contribution(s) is another quasi first-order relaxation that exhibits $^1/_e$ times typically in the range of ~ 0.5 to ~ 1 ps and is referred to as the intermediate component.[12,45] Rønne et al. accepted the proposal[12] that the intermediate component is coupled to orientational diffusion and that both response contributions originate in a single configurational coordinate. Therefore, the experimentally measured OHD-RIKES data for benzene ($T(\tau)$) were modified by subtraction of these response contributions at each temperature.[18] An alternate interpretation of the intermediate component of $R^{(3)}_{\text{eff}}(\tau)$ proposes that the subpicosecond, quasi first-order relaxation is inseparable from the higher-frequency vibrational dynamics at times $<2-3$ ps and originates in the correlation time of the intermolecular potential.[14] Within this model, the OHD-RIKES response function $R^{(3)}_{\text{eff}}(\tau)$ for a single vibrational mode is given by an inhomogeneously broadened coordinate[14,46]

$$R^{(3)}_{\text{vib}}(t) = \int_0^\infty \mathrm{d}\omega_i \, g(\omega_i) \, r^{(3)}_{\text{vib}}(\omega_i, t) \tag{16a}$$

where

$$r^{(3)}_{\text{vib}}(\omega_i, t) = \frac{\alpha_1^{\,2}}{2m\omega_i} \mathrm{e}^{-\Gamma t} \sin(\omega_i t) \tag{16b}$$

In eqs 16a and 16b, $r^{(3)}_{\text{vib}}(\omega_i, t)$ is a quantum harmonic oscillator response function with a homogeneous damping rate Γ and an inhomogeneous frequency distribution $g(\omega_i)$. For low-frequency oscillators, the rate parameters are commensurable and $\omega_j \cong \Gamma \cong \Delta\omega_j$, where $\Delta\omega_j$ is the width of the inhomogeneous frequency distribution. We have shown[14] that when the parameters of eqs 16a and 16b satisfy these relations, the tail of the vibrational response function exhibits the relaxation signature of the intermediate component. Additionally, the apparent $^1/_e$ time of the "decay" cannot be directly traced to the parameter Γ in eq 16b; the 0.45-ps $^1/_e$ time seen in our benzene data is reproduced by $\Gamma^{-1} = 1.44$ ps when eqs 16a and 16b are fit to the OHD-RIKES data of benzene at 24 °C. The apparent $^1/_e$ time is significantly shorter than the structural correlation time in part because of the additional interference effect due to coherent superposition in the integral of eq 16a. From this perspective, the intermediate component is intrinsic to the low-frequency vibrational coordinates and not physically separable from them. Although orientational diffusion is certainly a significant contribution to the potential fluctuation, the time constant Γ does not match either the collective or single-particle orientational correlation time for benzene (2.55 and ~ 2.43 ps[47]). Intermolecular translational motions would also contribute to potential fluctuations, and their inclusion may account for the small difference ($<2\times$) in the rate constants.

References and Notes

(1) Castner, E. W., Jr.; Maroncelli, M. *J. Mol. Liq.* **1998**, *77*, 36.
(2) Dalton, L. R.; Steier, W. H.; Robinson, B. H.; Zhang, C.; Ren, A.; Garner, S.; Chen, A.; Londergan, T.; Irwin, L.; Carlson, B.; Fifield, L.; Phenlan, G.; Kincaid, C.; Amend, J.; Jen, A. *J. Mater. Chem.* **1999**, *9*, 1905.
(3) Prevosto, D.; Bartolini, P.; Torre, R.; Capaccioli, S.; Ricci, M.; Taschin, A.; Pisignano, D.; Lucchesi, M. *Philos. Mag. B* **2002**, *82*, 553.
(4) (a) Laaksonen, A.; Stilbs, P.; Wasylishen, R. E. *J. Chem. Phys.* **1998**, *108*, 455. (b) Bauer, D. R.; Alms, G. R.; Brauman, J. I.; Pecora, R. *J. Chem. Phys.* **1974**, *61*, 2255.
(5) (a) Alms, G. R.; Bauer, D. R.; Brauman, J. I.; Pecora, R. *J. Chem. Phys.* **1973**, *58*, 5570. (b) Bartoli, F. J.; Litovitz, T. A. *J. Chem. Phys.* **1972**, *56*, 404.
(6) Kim, S. K.; Fleming, G. R. *J. Phys. Chem.* **1988**, *92*, 2168.
(7) Todd, D. C.; Jean, J. M.; Rosenthal, S. J.; Ruggiero, A. J.; Yang, D.; Fleming, G. R. *J. Chem. Phys.* **1990**, *93*, 8658.
(8) Smith, N. A.; Meech, S. R. *Int. Rev. Phys. Chem.* **2002**, *21*, 75.

(9) Lotshaw, W. T.; McMorrow, D.; Thantu, N.; Melinger, J. S.; Kitchenham, R. *J. Raman Spectrosc.* **1995**, *26*, 571.
(10) Cang, H.; Novikov, V. N.; Fayer, M. D. *J. Chem. Phys.* **2003**, *118*, 2800.
(11) Palese, S.; Mukamel, S.; Miller, R. J. D.; Lotshaw, W. T. *J. Phys. Chem.* **1996**, *100*, 10380.
(12) Loughnane, B. J.; Scodinu, A.; Farrer, R. A.; Fourkas, J. T.; Mohanty, U. *J. Chem. Phys.* **1999**, *111*, 2686.
(13) McMorrow, D.; Thantu, N.; Melinger, J. S.; Kim, S. K.; Lotshaw, W. T. *J. Phys. Chem.* **1996**, *100*, 10389.
(14) McMorrow, D.; Thantu, N.; Kleiman, V.; Melinger, J. S.; Lotshaw, W. T. *J. Phys. Chem. A* **2001**, *105*, 7960.
(15) Gottke, S. D.; Brace, D. D.; Cang, H.; Bagchi, B.; Fayer, M. D. *J. Chem. Phys.* **2002**, *116*, 360.
(16) Le Calvez, A.; Montant, S.; Freysz, E.; Ducasse, A.; Zhuang, X. W.; Shen, Y. R. *Chem. Phys. Lett.* **1996**, *258*, 620.
(17) Beard, M. C.; Turner, G. M.; Schmuttenmaer, C. A. *J. Phys. Chem. B* **2002**, *106*, 7146.
(18) Rønne, C.; Jensby, K.; Loughnane, B. J.; Fourkas, J.; Faurskov Nielsen, O.; Keiding, S. R. *J. Chem. Phys.* **2000**, *113*, 3749.
(19) Nymand, T. M.; Rønne, C.; Keiding, S. R. *J. Chem. Phys.* **2001**, *114*, 5246.
(20) Gerard, G.; Wynne, K. *J. Chem. Phys.* **2003**, *119*, 11753.
(21) *CRC Handbook of Chemistry and Physics*, 67th ed.; CRC Press Inc.: Boca Raton, FL, 1987.
(22) Certain commercial equipment, instruments, or materials are identified in this paper to specify adequately the experimental procedures. In no case does such identification imply a recommendation or endorsement by NIST or NRL nor does it imply that the materials or equipment identified are necessarily the best available for the described procedures.
(23) Lu, Z. G.; Campbell, P.; Zhang, X. C. *Appl. Phys. Lett.* **1997**, *71*, 593.
(24) Press: W. H.; Teukolsky, S. A.; Vetterling, W. T.; Flannery, B. P. *Numerical Recipes in Fortran*, 2nd ed.; Cambridge University Press: New York, , 1986.
(25) Staver, P. R.; Lotshaw, W. T. OSA Proceedings on *Advanced Solid State Lasers* **1994**, *20*, 252; Fan, T. Y.; Chai, B. H. T., Eds., Optical Society of America: Washington, DC, 1994.
(26) McMorrow, D.; Lotshaw, W. T. *J. Phys. Chem.* **1991**, *95*, 10395.
(27) Hellwarth, R. W. *Prog. Quantum Electron.* **1977**, *5*, 1.
(28) Chang, Y. C.; Castner, E. W., Jr. *J. Phys. Chem*. **1996**, *100*, 3330.
(29) Palese, S.; Schilling, L.; Miller, R. J. D.; Staver, P. R.; Lotshaw, W. T. *J. Phys. Chem.* **1994**, *98*, 6308.
(30) Chang, Y. J.; Castner, E. W., Jr. *J. Chem. Phys.* **1993**, *99*, 7289.
(31) Kinoshita, S.; Kai, Y.; Yamaguchi, M.; Yagi, T. *Chem. Phys. Lett.* **1995**, *236*, 259.
(32) Faurskov Nielsen, O. *Annu. Rep. Prog. Chem., Sect. C: Phys. Chem.* **1996**, *93*, 57.
(33) Bucaro, J. A.; Litovitz, T. A. *J. Chem. Phys.* **1971**, *54*, 3846.
(34) Mukamel, S. *Principles of Nonlinear Optical Spectroscopy*; Oxford University Press: New York, 1995.
(35) The OHD-RIKES experimental techniques and data reduction methods that we have employed and described in refs 9, 14, 26, 30, and 35 have consistently resulted in the ability to determine the decay constants for the orientational diffusion coordinate (τ_{or}) with a statistical accuracy no lower than $\pm$5%, and accuracies of $\pm$1$-$2% being common. By "well separated" we mean $^1/_e$ time constants that differ on the order of 2X.
(36) McMorrow, D.; Lotshaw, W. T.; Kenney-Wallace, G. A. *IEEE J. Quantum Electron.* **1988**, *24*, 443.
(37) McMorrow, D.; Lotshaw, W. T. *Chem. Phys. Lett*. **1993**, *201*, 369.
(38) At the GE Global Research Center, Niskayuna, NY, and the Naval Research Laboratory, Washington, DC.
(39) Neelakandan, M.; Pant, D.; Quitevis, E. L. *Chem. Phys. Lett.* **1997**, *265*, 283. Cong, P.; Deuel, H. P.; Simon, J. D. *Chem. Phys. Lett*. **1995**, *240*, 72.
(40) Beard, M. C.; Lotshaw, W. T.; McMorrow, D.; Heilweil, E. J., to be submitted for publication.
(41) Bertie, J. E.; Keefe, C. D. *J. Mol. Struct.* **2004**, *695*$-$*696C*, 39, data used by permission.
(42) Friedman, J. S. Ph.D. Dissertation, Colorado State University, 1992.
(43) Vanden Bout, D.; Muller, L. J.; Berg, M. *Phys. Rev. Lett.* **1991**, *67*, 3700.
(44) Steffen, T.; Meinders, N. A. C.; Duppen, K. *J. Phys. Chem.* **1998**, *102*, 4213.
(45) Lotshaw, W. T.; McMorrow, D.; Kalpouzos, C.; Kenney-Wallace, G. A. *Chem. Phys. Lett.* **1987**, *136*, 323.
(46) Steffen, T.; Fourkas, J. T.; Duppen, K. *J. Chem. Phys.* **1996**, *105*, 7364.
(47) The single-particle correlation time is calculated using our measured value for the collective correlation (τ_{or}) and the ratio of the static and dynamic structure factors used in ref 12.